Journal of Solid State Chemistry 187 (2012) 200–207

Contents lists available at SciVerse ScienceDirect

Journal of Solid State Chemistry

journal homepage: www.elsevier.com/locate/jssc

The polygallides: $Yb_3Ga_7Ge_3$ and $YbGa_4Ge_2$

Sebastian C. Peter [a,b], Christos D. Malliakas [a], Heinze Nakotte [c,d], Karunakar Kothapilli [c,d], Sudhindra Rayaprol [e], Arthur J. Schultz [f], Mercouri G. Kanatzidis [a,g,*]

[a] Department of Chemistry, Northwestern University, 2145N. Sheridan Road, Evanston, IL 60208, USA
[b] New Chemistry Unit, Jawaharlal Nehru Centre for Advanced Scientific Research, Jakkur, Bangalore 560064, India
[c] Physics Department, New Mexico State University, Las Cruces, NM 88003, USA
[d] Los Alamos Neutron Science Center, Los Alamos National Laboratory, Los Alamos, NM 87545, USA
[e] UGC-DAE Consortium for Scientific Research, Mumbai Centre, BARC, R-5 Shed, Trombay, Mumbai 400085, India
[f] X-Ray Science Division, Argonne National Laboratory, Argonne, IL 60439, USA
[g] Materials Science Division, Argonne National Laboratory, Argonne, IL 60439, USA

ARTICLE INFO

Article history:
Received 26 November 2011
Received in revised form
30 December 2011
Accepted 2 January 2012
Available online 14 January 2012

Keywords:
Intermetallics
Metal flux synthesis
Crystal structure
Neutron diffraction
Magnetism

ABSTRACT

$Yb_3Ga_7Ge_3$ and $YbGa_4Ge_2$ were obtained from reactions of Yb and Ge in excess liquid gallium. The crystal structure of $Yb_3Ga_7Ge_3$ was refined using X-ray and neutron diffraction data on selected single crystals. $Yb_3Ga_7Ge_3$ crystallizes in the monoclinic space group $C2/c$ with lattice constants $a=12.2261(20)$ Å, $b=10.7447(20)$ Å, $c=8.4754(17)$ Å and $\beta=110.288(30)^\circ$ (neutron diffraction data). The crystal structure of $Yb_3Ga_7Ge_3$ is an intergrowth of planar layers of $YbGa_xGe_y$ and puckered layers of $(Ge)_n$. $YbGa_4Ge_2$ crystallizes in a modified $PuGa_6$ structure type in the tetragonal polar space group $I4cm$ with lattice constants $a=b=5.9874(6)$ Å and $c=15.1178(19)$ Å. The structure of $YbGa_4Ge_2$ is an intergrowth of puckered Ga layers and puckered Ga_xGe_y layers with Yb atoms residing within the channels formed by the connection of the two layers. Physical properties, resistivity (ρ), magnetic susceptibility (χ) and specific heat (C) were measured for $Yb_3Ga_7Ge_3$. No magnetic ordering was observed. It was found that at low temperatures, ρ varied as T^2 and $C \propto T$, indicating Fermi-liquid regime in $Yb_3Ga_7Ge_3$ at low temperatures.

1. Introduction

In recent years the use of molten fluxes as reactive solvents for the discovery synthesis of intermetallic compounds has proven to be an excellent approach and has produced many novel ternary and quaternary intermetallic phases [1–9]. Several new pollygallides with an impressive set of diverse structures and compositions have been synthesized using Ga as solvent [10–27]. Examples include $Yb_2Ga_4Ge_6$ [11], $Yb_3Ga_4Ge_6$ [11], $Eu_3Ga_4Ge_6$ [11], Sm_2NiGa_{12} [12], $RERu_2Ga_8$ [15], $RE_2Ru_3Ga_{10}$ [15], RE_3Ga_9Ge (RE=Y, Ce, Sm, Gd, Yb) [20], $RE_2Ru_3Ga_9$ [21], $RE_{1.34}Pt_4Ga_{10}$ [16], RE_2NiGa_{10} (RE=La, Ce) [17], RE_3NiGa_{10} (RE=Ce, Pr, Nd) [18] and $Ce_3Ni_2Ga_{15}$ [19] and quaternary compounds $RE_4FeGa_{12-x}Ge_x$ ($x=2.5$) [23], $RE_{0.67}M_2Ga_{5+n-x}Ge_x$ ($n=0$, 1; $x=0.67$; RE=Sm, Gd-Tm) [24], $REMGa_3Ge$ (RE=Y, Sm, Tb, Gd, Er, Tm; M=Ni, Co) [26], $RE_3Ni_3Ga_8Ge_3$ (RE=Sm, Gd) [26] and $YCo_{0.88}Ga_3Ge$ [27]. Among rare earths, the Yb-containing compounds have particular scientific interest because they can exhibit two energetically similar electronic configurations: the magnetic Yb^{3+} ($4f^{13}$) and the nonmagnetic Yb^{2+} ($4f^{14}$) one. Due to this feature Yb is usually considered as the "*f*-hole" analog of Ce. In this case, the roles of the 4*f* electron and 4*f* hole can be interchanged, and many phenomena, such as intermediate valence, Kondo effect or heavy-fermion behavior, are observed in Ce and Yb analogs [28–30].

Four compounds have been reported in the Yb–Ga–Ge system. The equiatomic compound YbGaGe [31], when doped [32], exhibits anomalous thermal expansion properties and crystallizes in the hexagonal $P6_3/mmc$ space group. Yb_3Ga_9Ge [20] adopts the Ce_3Ga_9Ge type structure with an open Ga framework containing straight parallel tunnels. $Yb_2Ga_4Ge_6$ crystallizes in the polar orthorhombic $Cmc2_1$ space group while $Yb_3Ga_4Ge_6$ adopts the monoclinic $C2/m$ space group [11]. Both structures were described on the basis of the Zintl concept of bonding, in which the three-dimensional $[Ga_4Ge_6]^{n-}$ framework serves as a host and electron sink for the electropositive Yb atoms. One challenge in these types of compounds is the difficulty in distinguishing between the Ga and Ge atoms using X-ray diffraction data because of the very small difference in scattering power. In some cases it is possible to do so on the basis of reasonable bond lengths coupled with elemental analysis results. In other cases neutron diffraction (ND) analysis can help because of the small but significant difference in scattering length between Ga and Ge.

* Corresponding author at: Department of Chemistry, Northwestern University, 2145N. Sheridan Road, Evanston, IL 60208, USA. Fax: +1 847 491 5937.
E-mail address: m-kanatzidis@northwestern.edu (M.G. Kanatzidis).

0022-4596/$ - see front matter © 2012 Elsevier Inc. All rights reserved.
doi:10.1016/j.jssc.2012.01.006

Here, we describe $Yb_3Ga_7Ge_3$ and $YbGa_4Ge_2$, two new members of the Yb/Ga/Ge family. The crystal structure of $Yb_3Ga_7Ge_3$ was refined using X-ray single crystal data and the Ga/Ge atomic site differentiation was investigated with single crystal neutron diffraction measurements on a large single crystal. A structural comparison between $Yb_3Ga_7Ge_3$ and other related compounds within the Yb–Ga–Ge system is presented. $YbGa_4Ge_2$ crystallizes in a modified $PuGa_6$ structure type adopting the rare polar space group *I*4*cm*. Magnetic susceptibility studies on $Yb_3Ga_7Ge_3$ show that it is an intermediate/mixed Yb valent compound exhibiting a magnetic transition associated with a Yb^{2+} to Yb^{3+} valence change. Resistivity and heat capacity measurements for $Yb_3Ga_7Ge_3$ indicate Fermi liquid metallic behavior and there are indications of valence fluctuations of Yb atoms.

2. Experimental

2.1. Synthesis

Compounds $Yb_3Ga_7Ge_3$ and $YbGa_4Ge_2$ were discovered in reactions containing Pd. Molten Ga was used as a solvent for the synthesis of both compounds. Yb (in the form of powder ground from metal chunks, 99.9%, Chinese Rare Earth Information Center, Inner Mongolia, China), Pd pieces (99.99%, American elements, CA), Ga (3 mm shots 99.999%, CERAC Inc.) and germanium pieces (99.999%, Plasmaterials, Livermore, CA) were used as obtained.

$Yb_3Ga_7Ge_3$ and $YbGa_4Ge_2$ were obtained by combining ytterbium, palladium, gallium and germanium in the 3:2:30:6 atomic ratio. An amount of 300 mg of Yb, 123 mg of Pd, 1.208 g of Ga and 251.8 mg of Ge were used as starting materials. The starting elements were loaded into alumina crucibles in a nitrogen filled glove-box. The crucibles were placed into fused silica tubes and evacuated to approximately 7×10^{-4} Torr. The tubes were then placed in a furnace and treated with the following heating profile: the temperature was raised to 1273 K at 100 K/h and held at 1273 K for 5 h to ensure a proper melt, the furnace was then cooled to 1123 K in 2 h and kept isothermally at 1123 K for 48 h, and then cooled to 373 K at 100 K/min. Excess Ga was removed in a two-step process: first by hot-temperature spin-filtration, forcing liquid Ga through specially designed screen filters by centrifuging at high speed (4300 rpm) for approximately 30 s, and second by treating the product with a $\sim$3 M solution of I_2 in dimethylformamide (DMF) for 12–24 h. The product was subsequently rinsed with DMF, hot water, and dried with acetone and ether. The product mixture contains large (2–3 mm length) $Yb_3Ga_7Ge_3$ single crystals as the major phase, a few small single crystals of $YbGa_4Ge_2$ and recrystallized Ge. The resultant crystalline products possessed needle to bar-like morphology and typical metallic luster. In some cases aggregation of needles into bundles was observed.

The specific synthesis conditions under which $YbGa_4Ge_2$ was discovered appear to be essential for its stabilization. Several direct attempts made to synthesize $YbGa_4Ge_2$ in bulk by varying the starting composition (including gallium+indium flux) and using various techniques such as arc-melting and high frequency induction heating were unsuccessful. The main products observed from these experiments (Powder XRD pattern is available in supporting information) were the more thermodynamically stable YbGaGe [31] and $YbGa_2$ [33].

2.2. Powder X-ray diffraction

Phase identity and purity of the $Yb_3Ga_7Ge_3$ sample was determined by powder XRD experiments that were carried out on an Inel diffractometer using Cu*K*α radiation. The experimental powder pattern was compared to patterns calculated from the single crystal structure refinement.

2.3. Elemental analysis

Quantitative microprobe analyses of the compounds were performed with a Hitachi S-3400 scanning electron microscope (SEM) equipped with a PGT energy dispersive X-ray analyzer. Data were acquired with an accelerating voltage of 20 kV and a 60 s accumulation time. The EDS analyses taken on visibly clean surfaces of $Yb_3Ga_7Ge_3$ crystals gave the atomic composition of 23($\pm$1)% Yb, 54($\pm$1)% Ga and 23($\pm$1)% Ge, which is in very good agreement with the results derived from the single crystal X-ray and neutron diffraction refinements. For $YbGa_4Ge_2$ single crystals, the EDS analysis gave the atomic composition of 14($\pm$1)% Yb, 57($\pm$1)% Ga and 29($\pm$1)% Ge is fairly good agreement with the single crystal X-ray diffraction results gave atomic compositions in good agreement. EDS data were acquired using 1 min exposure time. The presence of Pd in both compounds was ruled out by increasing the exposure time of the beam to more than 5 min.

2.4. Single crystal X-ray diffraction

The X-ray intensity data of $Yb_3Ga_7Ge_3$ and $YbGa_4Ge_2$ were collected at room temperature using a STOE IPDS 2 T diffractometer with graphite-monochromatized Mo*K*α (λ=0.71073 Å) radiation. The X-AREA (X-RED and X-SHAPE within) package suite [34] was used for the data extraction, integration and application of analytical absorption corrections. The structures of $Yb_3Ga_7Ge_3$ and $YbGa_4Ge_2$ were solved by direct methods and refined using JANA2006 [35] with anisotropic displacement parameters for all atoms.

Initial indexing of the X-ray diffraction data of $Yb_3Ga_7Ge_3$ provided the lattice constants a=12.219(1) Å, b=10.737(1) Å, c=8.4708(8) Å, β=110° with a monoclinic *Cc* space group. The refinement converged to the residuals $R1$=0.068 and $wR2$=0.128. However, the presence of a center of symmetry observed in the structure and the experimental $[E^2-1]$ value (0.899) close to the theoretical centrosymmetric value (0.968) pointed towards a centrosymmetric space group. In the next step, we considered the *C*2/*c* space group and refined the crystal structure successfully. The asymmetric unit of $Yb_3Ga_7Ge_3$ contains a total of eight atomic positions. Two Yb atoms reside at 4*e* and 8*f* positions and the other six positions (two 4*e* and four 8*f*) are shared by Ga and Ge atoms. The refinement converged to the residuals $R1$=0.0508 and $wR2$=0.1235. Due to the very small difference in X-ray scattering it is difficult to distinguish between the Ga and Ge atoms. Another attempt to distinguish Ga and Ge was done on the basis of bond distances but was inconclusive. Except for Yb-(Ge/Ga)(2) (3.202(2) Å), all other Yb-(Ge/Ga) bond distances are within a small range (3.0494(13)–3.1038(15) Å). The final refinement of $Yb_3Ga_7Ge_3$ was done on the basis of the available single crystal neutron diffraction.

Successful refinement for $YbGa_4Ge_2$ was accomplished only in the polar tetragonal space group *I*4*cm*. ND data could not be obtained to differentiate the Ga and Ge atoms due to the small size of the single crystals. Structure refinement, however, was successfully done on the basis of bond lengths and consistency with EDS elemental analysis, as done in previous works [11,20]. The shortest bond to Yb in $YbGa_4Ge_2$ is 3.052(6) Å and was assigned as Yb–Ge because Ge has a smaller covalent radius (1.22 Å) compared to Ga (1.26 Å). A total of five atomic positions were observed in the asymmetric unit of $YbGa_4Ge_2$. The Yb atom resides at the 4*b* position, the three Ga atoms occupy 4*a* and 8*c* sites, and the Ge atom is found at 8*c*. The refinement of Ge and

Ga(1) positions resulted in slightly enlarged isotropic displacement parameters (U_{eq} is $20(1)\times10^{-3}$ and $21(1)\times10^{-3}$ Å^2 for Ge and Ga(1), respectively) but the refinement converged to the acceptable residuals of $R1=0.0469$ and $wR2=0.1255$. An attempt to mix the Ga and Ge positions did not help lower the isotropic displacement parameters for Ga(1) and Ge atoms. The details of the data collection and crystallographic refinement of $YbGa_4Ge_2$ are given in Table 1. A list of atomic positions, isotropic displacement parameters and bond distances are shown in Tables 2 and 3. The anisotropic displacement parameters of $YbGa_4Ge_2$ are available in supporting information.

Table 1
Crystal data and details of structure refinement for $YbGa_4Ge_2$ and $Yb_3Ga_7Ge_3$. Further details on the structure refinements are available[a].

Molecular formula	$YbGa_4Ge_2$	$Yb_3Ga_7Ge_3$
Diffraction method	X-ray	Neutron
Formula weight	597.1	1227.48
Temperature	293(5)	298 K
Space group	*I*4*cm*	*C*2/*c*
a (Å)	5.9874(6)	12.2261(20)
b (Å)	5.9874(6)	10.7447(20)
c (Å)	15.1178(19)	8.4754(17)
β (deg)	90	110.288(30)
V (Å^3)	541.96(10)	1044.3(4)
Z	4	4
ρ (g cm^{-3})	7.3156	7.868
Data collection technique		time-of-flight Laue
μ	47.428 mm^{-1}	$0.565+0.275\,\lambda$ cm^{-1}
Reflections collected	1642	896
Parameters	23	84
R_1[b] [$I>2\sigma(I)$], wR_2[c]	0.0476, 0.1395	
R indices $R_w(F^2)$[d], $R(F^2)$[e]		0.096, 0.149
R indices $R_w(F)$[f], $R(F)$[g]		0.047, 0.089

[a] Details may be obtained from: Fachinformationszentrum Karlsruhe, D-76344 Eggenstein-Leopoldshafen (Germany), by quoting the Registry No's. CSD– 423995 ($Yb_3Ga_7Ge_3$) and CSD– 423996 ($YbGa_4Ge_2$).
[b] $R=\sum\|F_o|-|F_c\|/\sum|F_o|$, $wR=\{\sum[w(|F_o|^2-|F_c|^2)^2]/\sum[w(|F_o|^4)]\}b^{1/2}$.
[c] $w=1/(\sigma^2(I)+0.0016I^2)$.
[d] $R_w(F^2)=\{\sum[w(F_o^2-F_c^2)^2]/\sum[w(F_o^2)^2]\}^{1/2}$.
[e] $R(F^2)=\sum|F_o^2-F_c^2|/\sum|F_o^2|$.
[f] $R_w(F)=\{\sum[w(F_o-F_c)^2]/\sum[w(F_o)^2]\}^{1/2}$.
[g] $R(F)=\sum|F_o-F_c|/\sum|F_o|$.

Table 2
Atomic coordinates ($\times10^4$) and equivalent isotropic displacement parameters (Å$^2\times10^3$) for $YbGa_4Ge_2$ at 293(5) K with estimated standard deviations in parentheses.

Label	Wyckoff site	*x*	*y*	*z*	Occupancy	U_{eq}[a]
Yb	4*b*	5000	0	5823.15	1	6(1)
Ge	8*c*	3383(4)	8383(4)	4018(5)	1	22(1)
Ga(1)	8*c*	2121(5)	7121(5)	2539(4)	1	19(1)
Ga(2)	4*a*	0	0	9953(4)	1	9(2)
Ga(3)	4*a*	0	0	1586(5)	1	10(2)

[a] U_{eq} is defined as one-third of the trace of the orthogonalized U_{ij} tensor.

Table 3
Selected bond lengths (Å) for $YbGa_4Ge_2$ at 298 K with estimated standard deviations in parentheses.

Atoms	Distance (Å)	Atoms	Distance (Å)
Yb–Ge × 2	3.054(7)	Ge–Ga(1)	2.478(9)
Yb–Ga(1) × 2	3.155(5)	Ge–Ga(1) × 2	3.178(7)
Yb–Ga(2) × 4	3.270(2)	Ge–Ga(2) × 2	2.653(6)
Yb–Ga(3) × 4	3.208(3)	Ga(1)–Ga(1) × 4	3.028(5)
Ge-Ge	2.738(4)	Ga(1)–Ga(3) × 2	2.581(6)

2.5. Single crystal neutron diffraction

ND data on $Yb_3Ga_7Ge_3$ were obtained at the Lujan Neutron Scattering Center at Los Alamos National Laboratory using the time-of-flight Laue single-crystal diffractometer (SCD) [36]. The description of the instrument [36] and details of the data collection and analysis procedures have been published previously [37]. Refinement of the neutron structure confirmed our original X-ray refinement model (including bond distances).

At the Lujan Neutron Scattering Center, pulses of protons are accelerated into a tungsten target at a frequency of 20 Hz to produce pulses of neutrons by means of the spallation process. The SCD on FP6 views a room temperature water moderator with a moderator-to-sample distance of 755 cm. Exploiting the pulsed nature of the source, neutron wavelengths are determined by time-of-flight based on the de Broglie equation $\lambda=(h/m)(t/l)$, where *h* is Planck's constant, *m* is the neutron mass and *t* is the time-of-flight for a flight path *l*, so that the entire thermal spectrum of neutrons can be employed. Using position-sensitive area detectors and a range of neutron wavelengths, a solid volume of reciprocal space is sampled with each stationary orientation of the sample and the detectors. The SCD has two ^{6}Li-glass scintillation position-sensitive area detectors, each with an active area of 15×15 cm^2 and a spatial resolution of 1.5 mm. The detectors are centered at scattering angles of 75° and 120° and with crystal-to-detector distances of 23 and 18 cm, respectively.

A crystal of $Yb_3Ga_7Ge_3$, with an approximate volume of 0.55 mm^3, was glued to an aluminum pin that was mounted on the SCD diffractometer. For each setting of the diffractometer χ and φ angles, data were stored in three-dimensional histogram form with coordinates *x*, *y*, *t* corresponding to horizontal and vertical detector positions and the time-of-flight, respectively. Data were analyzed using the ISAW software package in addition to other local SCD programs [38]. Bragg peaks in the recorded histograms were integrated about their predicted locations and were corrected for the Lorentz factor, the incident spectrum and the detector efficiency. A wavelength-dependent spherical absorption correction was applied using cross-sections from Sears [39] ($\mu(\text{cm}^{-1})=0.565+0.275\lambda$). Symmetry-related reflections were not averaged since different extinction factors are applicable to reflections measured at different wavelengths.

The GSAS software package was used for structural analysis [40]. The atomic positions of the X-ray diffraction structure were used as a starting point in the refinement. The refinement was based on F^2 reflections with a minimum *d*-spacing of 0.7 Å for the neutron data. Weights were assigned as $w(F_o^2)=1/[(\sigma(F_o^2)]^2$ where $\sigma^2(F_o^2)$ is the variance based on counting statistics. Data collection for the neutron diffraction data is summarized in Table 1. The refinement parameters and the selected bond distances are given in Tables 4 and 5. The anisotropic displacement parameters are available in supporting information.

Table 4
Atomic coordinates ($\times10^4$) for $Yb_3Ga_7Ge_3$ obtained from the single crystal neutron diffraction refinement. The mixed sites of Ga and Ge are represented as Ge sites (Ge(1), Ge(2) and Ge(3)) because Ge is the strong scatterer in neutron diffraction. Occupancy of mixed sites corresponds to the gallium atoms.

Atom	Wyckoff site	*x*	*y*	*z*	Occupancy
Yb1	8*f*	1914(3)	1(2)	956(2)	1
Yb2	4*e*	0	7130(3)	2500	1
Ga1	8*f*	56(5)	1940(3)	930(4)	1
Ga2	4*e*	0	4151(4)	2500	1
Ge1	8*f*	1140(4)	5003(3)	574(4)	0.911(16)
Ge2	8*f*	2038(4)	2888(3)	1050(4)	0.903(15)
Ge3	8*f*	1951(4)	7147(3)	945(4)	0.975(15)
Ge4	4*e*	5000	4957(3)	2500	1

Table 5
Selected bond lengths (Å) for $Yb_3Ga_7Ge_3$ at 298 K with estimated standard deviations in parentheses as obtained from the single crystal neutron diffraction refinement.

Atoms	Distance (Å)	Atoms	Distance (Å)
Yb(1)–Ga(1)	3.077(5)	Yb(2)–Ge(2)	3.172(4)
Yb(1)–Ga(1)	3.168(5)	Yb(2)–Ge(2)	3.494(5)
Yb(1)–Ga(2)	3.6544(32)	Yb(2)–Ge(3)	3.100(4)
Yb(1)–Ge(1)	3.075(5)	Yb(2)–Ge(4)	3.038(5)
Yb(1)–Ge(2)	3.1050(33)	Ga(1)–Ga(1)	2.713(6)
Yb(1)–Ge(2)	3.314(4)	Ga(1)–Ga(2)	2.735(5)
Yb(1)–Ge(2)	3.3446(34)	Ga(1)–Ge(2)	2.597(7)
Yb(1)–Ge(3)	3.0671(32)	Ga(1)–Ge(3)	2.609(7)
Yb(1)–Ge(3)	3.407(4)	Ga(1)–Ge(4)	2.525(4)
Yb(1)–Ge(3)	3.3760(34)	Ga(2)–Ge(1)	2.650(4)
Yb(1)–Ge(4)	3.0525(25)	Ge(1)–Ge(1)	2.614(9)
Yb(1)–Ge(4)	3.0506(27)	Ge(1)–Ge(2)	2.495(4)
Yb(2)–Ga(1)	3.0519(32)	Ge(1)–Ge(3)	2.485(4)
Yb(2)–Ga(2)	3.201(5)	Ge(2)–Ge(2)	2.556(6)
Yb(2)–Ge(1)	3.377(4)	Ge(2)–Ge(3)	2.543(4)
Yb(2)–Ge(1)	3.3857(35)	Ge(3)–Ge(3)	2.537(6)

ND data refinements show that Yb(1), Yb(2), Ga(1), Ga(2) and Ge(4) are fully occupied. The mixed sites of Ga and Ge are represented as Ge sites (Ge(1), Ge(2) and Ge(3)) because Ge is the strong scatterer in neutron diffraction. The composition obtained from the ND refinement is in good agreement with the composition indicated by the EDS analysis. In order to evaluate the Ga/Ge ratio on the 6 sites assigned to these atoms, the atom type for all 6 sites was set to Ge (the stronger scatterer) and the fractional occupancy of each site was refined. The scattering lengths for Ga and Ge are $b_{Ga}=7.288$ and $b_{Ge}=8.185$ fm. The product of the "fractional occupancy," FRAC, times the scattering length, b_{Ge}, is the observed scattering length, b_{obs}, for that site, *assuming the site is fully occupied*. Then,

$$b_{obs} = x b_{Ga} + (1-x) b_{Ge} \quad \text{and} \quad x = (b_{Ge} - b_{obs})/(b_{Ge} - b_{Ga})$$

Refinement of independent occupancies resulted in a range of 0.868(21)–1.028(25), where a value of 0.890 is a fully occupied Ga site and 1.0 is a full occupied Ge site. Atoms Ga(1) and Ga(2) were close to fully occupied Ga and Ge(4) was close to fully occupied Ge, and were set to these values and their occupancies were not refined. The occupancies of atoms Ge(1), Ge(2) and Ge(3) were refined in the final model. From the above equations, the overall stoichiometry is Yb:Ga:Ge=3:6.85(20):3.15(9), or $Yb_3Ga_7Ge_3$ rounded off to the nearest integers.

2.6. Magnetism

Magnetization measurements for $Yb_3Ga_7Ge_3$ were conducted on selected single crystals using a Quantum Design MPMS SQUID magnetometer. Temperature dependence data were collected for both zero field cooled (ZFC) and field cooled mode (FC) between 2 and 300 K, with applied fields of 1 kG. The field-dependent magnetic measurements, conducted at 5 K, were carried out in fields up to $\pm$55 kG. A diamagnetic correction was applied to the data to account for the core diamagnetism.

2.7. Electrical resistivity

Electrical resistivity on selected crystals of $Yb_3Ga_7Ge_3$ was measured over the temperature range of 2–300 K using a four-probe dc technique with contacts made with silver paste. The measurements were conducted using a Quantum Design PPMS magnetometer.

2.8. Heat capacity

Heat capacity (C_p) measurements were performed on several single crystals of $Yb_3Ga_7Ge_3$ by the relaxation method using a QD-PPMS. The sample was adhered to a calibrated HC-puck using *Apiezon N* grease. C_p was measured in the 2–50 K range with no applied magnetic fields (H). The electronic and phonon contributions to the heat capacity were derived by fitting the C_p/T vs. T plot using the Debye function [41] within the temperature range 2–50 K.

3. Results and discussion

3.1. Reaction chemistry

The compounds $Yb_3Ga_7Ge_3$ and $YbGa_4Ge_2$ were obtained from reactions of Yb/Pd/Ge in liquid Ga. The new monoclinic phase of $Yb_3Ga_7Ge_3$ was isolated in high yield ($>90\%$), whereas the tetragonal phase $YbGa_4Ge_2$ was present in minor quantities. Powder XRD of ground single crystals of $Yb_3Ga_7Ge_3$ compared with simulated powder pattern obtained from the single crystal refinement is available in the supporting information. Attempts to synthesize $Yb_3Ga_7Ge_3$ starting from the ideal composition and in the absence of Pd favored the formation of the previously reported compound $Yb_3Ga_4Ge_6$ [11]. We did not observe crystals of $Yb_3Ga_7Ge_3$ from similar reactions with other transition metals such as Ru, Rh and Ag. We speculate that palladium could act as a nucleating agent for the formation of $Yb_3Ga_7Ge_3$ and $YbGa_4Ge_2$. The unreacted Pd was observed in the chunk left over after manually separating single crystals from the reaction mixture. A similar behavior was reported in the case of $Yb_5Al_2Sb_6$ [42] and $YbGe_{2.83}$ [43]. Other synthetic techniques such as arc melting, high frequency induction heating, and direct stoichiometric reaction in resistive furnaces also failed to produce the title compounds (Supporting information).

The single crystals of $Yb_3Ga_7Ge_3$ grow as metallic silver rods and appear to be stable in air indefinitely. SEM images of typical crystals of $Yb_3Ga_7Ge_3$ and $YbGa_4Ge_2$ as grown from the flux synthesis are shown in Fig. 1. Reaction byproducts were recrystallized germanium, $PdGa_5$ and a few polygonal-shaped crystals of $YbGa_4Ge_2$, which could be easily distinguished and removed when necessary. Fig. 1b depicts a SEM image of a typical single crystal of $YbGa_4Ge_2$.

3.2. Crystal structure

3.2.1. $Yb_3Ga_7Ge_3$

The structure of $Yb_3Ga_7Ge_3$ is closely related to that of Yb_3Ga_9Ge (Ce_3Ga_9Ge type), see Fig. 2a. $Yb_3Ga_7Ge_3$ crystallizes in the monoclinic $C2/c$ space group ($a=12.2261(20)$ Å, $b=10.7447(20)$ Å, $c=8.4754(17)$ Å and $\beta=110.288(30)^\circ$), which derives from the reduced orthorhombic cell of Yb_3Ga_9Ge

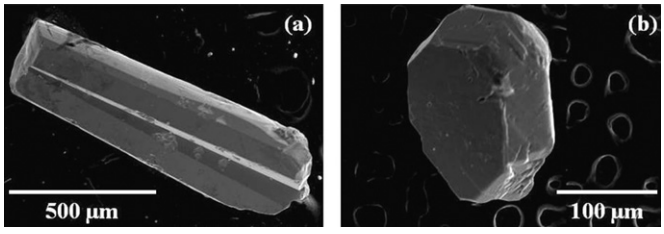

Fig. 1. SEM image of typical Ga flux grown crystals of (a) $Yb_3Ga_7Ge_3$ and (b) $YbGa_4Ge_2$.

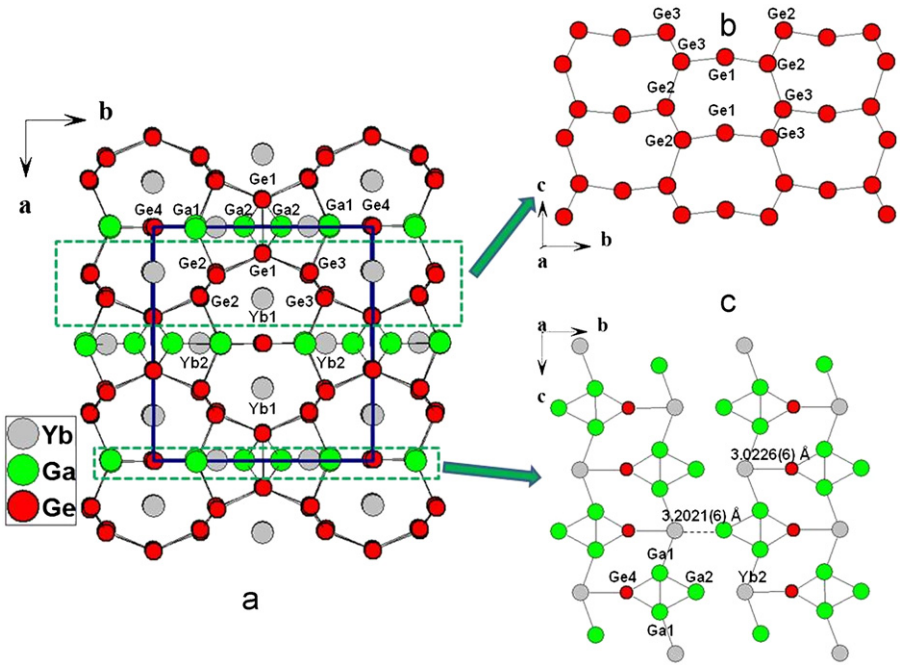

Fig. 2. (a) Projection of the structure of $Yb_3Ga_7Ge_3$ along the *c*-axis. Ge(1), Ge(2) and Ge(3) are Ga/Ge mixed positions and represented as Ge. (b) The two-dimensional puckered layer and (c) the Yb–Ga–Ge plane viewed along the *a*-axis.

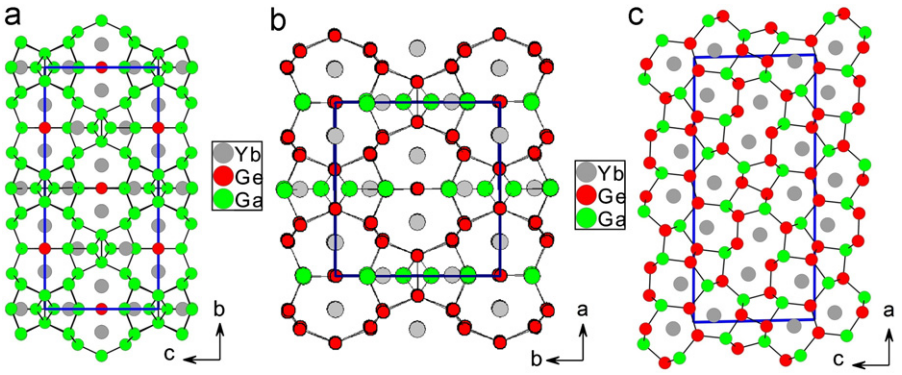

Fig. 3. Comparison of the three structures of $Yb_3Ga_9Ge_1$, $Yb_3Ga_7Ge_3$ and $Yb_3Ga_4Ge_6$. Ge(1), Ge(2) and Ge(3) in $Yb_3Ga_7Ge_3$ are Ga/Ge mixed positions and marked as Ge.

(a=8.5037(18) Å, b=23.007(4) Å, c=10.7860(3) Å) (Fig. 3a). The crystal structure of $Yb_3Ga_7Ge_3$ is complex featuring a three-dimensional (3D) framework of $[Ga_7Ge_3]^{n-}$ with Yb atoms filling the voids. For the sake of simplicity it is worthwhile to sub-divide the structure into 2 two-dimensional (2D) units: a puckered $(Ge)_n$ layer (Fig. 2b) and a planar $Yb(2)(GaGe)_n$ layer (Fig. 2c). These 2D motifs alternate along the *a*-axis and the Yb(1) atoms are inserted in the remaining voids. The puckered layer is made of 8-membered boat-shaped rings condensed into a 2D puckered layer by sharing all eight sides with adjacent rings. The planar layers are made up of Ga_3Ge_1 rhombic units interconnected with Yb(2) atoms. This planar layer is made of ribbons separated along the *b*-axis with Yb(2)–Ga(2) distances of 3.2021(6) Å. Alternatively, in both Yb_3Ga_9Ge and $Yb_3Ga_7Ge_3$ structures (Figs. 3a and 3b, respectively) the Ge atoms form puckered fragments, as shown in Fig. 4, which are connected side by side with other $(GaGe)_n$ fragments to form the 3D framework structure.

It is interesting to further compare the crystal structure of $Yb_3Ga_7Ge_3$ with $Yb_3Ga_4Ge_6$ [11] (Fig. 3). $Yb_3Ga_7Ge_3$ and $Yb_3Ga_4Ge_6$ have different Ga/Ge frameworks (Fig. 3b and c, respectively). In $Yb_3Ga_4Ge_6$, the framework forms different types of tunnels that are filled with Yb atoms except for the smaller five-membered tunnels. The average Ga–Ge distance of 2.623 Å in $Yb_3Ga_7Ge_3$ is slightly longer than those in Yb_3Ga_9Ge (2.57 Å) [20] and in $Yb_3Ga_4Ge_6$ (2.54 Å) [11].

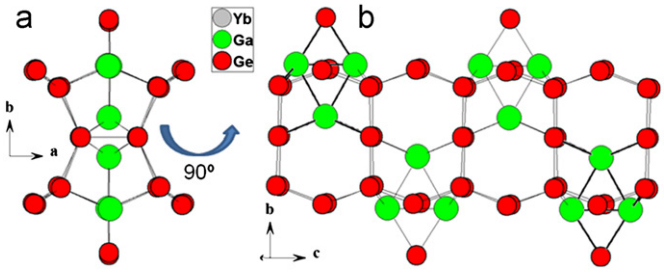

Fig. 4. (a) Column of Ga and Ge atoms from the structures of $Yb_3Ga_7Ge_3$ and $Yb_3Ga_9Ge_1$. (b) The ribbons are extended along the *a*-axis as zig-zag chains and coordinated to other ribbons.

The local coordination environments of the Yb atoms within a radius of 3.5 Å and of Ga and Ge atoms within 3.0 Å are presented

in supporting information. Both Yb atoms are coordinated with 12 Ga and Ge atoms, but the nature of the coordination spheres is different. Yb(1) has almost a spherical coordination sphere and Yb(2) has a butterfly-shaped coordination environment. The average Yb–Ga and Yb–Ge distances in the coordination environment for Yb(1) is 3.1737 Å and for Yb(2) is 3.245 Å. Considering the sum of single bonded metallic radii [44] for Yb (1.94 Å) and Ga (1.26 Å) these interactions could be regarded as fairly strong. The atoms within 3.0 Å of Ga and Ge result in irregular coordination that includes 2–6 other atoms. Ga(1) and Ga(2) have a penta-coordinated sphere. The mixed sites, Ge(1), Ge(2) and Ge(3) have a tetra-coordinated environment of Ga and Ge atoms and Ge(4) has only two Ga(1) atoms surrounding it.

3.2.2. $YbGa_4Ge_2$

The crystal structure of $YbGa_4Ge_2$ is closely related to that of $YbGa_6$ (tetragonal, $P4/nbm$) [45], which crystallizes in the $PuGa_6$ type structure. The *c*-axis is doubled in $YbGa_4Ge_2$ and the symmetry is lowered to the rare polar space group, $I4cm$ (Fig. 5). A projection of the $YbGa_4Ge_2$ structure onto the *ac* plane is presented in Fig. 5a. Bonds to the Yb atoms have been omitted to emphasize the 3D $[Ga_4Ge_2]$ framework and its channels. The polar axis coincides with the crystallographic *c*-axis. In $YbGa_4Ge_2$, all Yb, Ga and Ge atoms are grouped separately in alternating layers stacked along the *c*-axis in the sequence: Yb–Ga(2)–Ge–Ga(1)–Ga(3). The structure can also be described as an alternating stacking of puckered Ga layers (Fig. 5b) and puckered mixed Ga/Ge layers (Fig. 5c). The Yb atoms reside within the channels formed by the connection of the two layers.

In the puckered Ga layer, Ga(3) is coordinated with four Ga(1) atoms to form a distorted 2D sheet that extends in the *ab*-plane (Fig. 5b). The diatomic layer, on the other hand, is composed of Ga(2) and Ge atoms. In this layer, Ga(2) is coordinated to four Ge atoms and Ge is connected trigonally to two Ga(2) atoms and one Ge atom, respectively. The two layers, described above, are bridged by the Ga(2) and Ga(3) atoms along the *c*-axis thus building the 3D $[Ga_4Ge_2]$ open framework. The connection of the two layers via Ga(2)–Ga(1) bonds makes a 5 coordinate (4 Ge and 1 Ga(3)) distorted square pyramidal geometry for the Ga(2) atoms, and a 5 coordinate (4 Ga(1) and 1 Ga(2)) distorted square pyramidal geometry arrangement for the Ga(3) atoms.

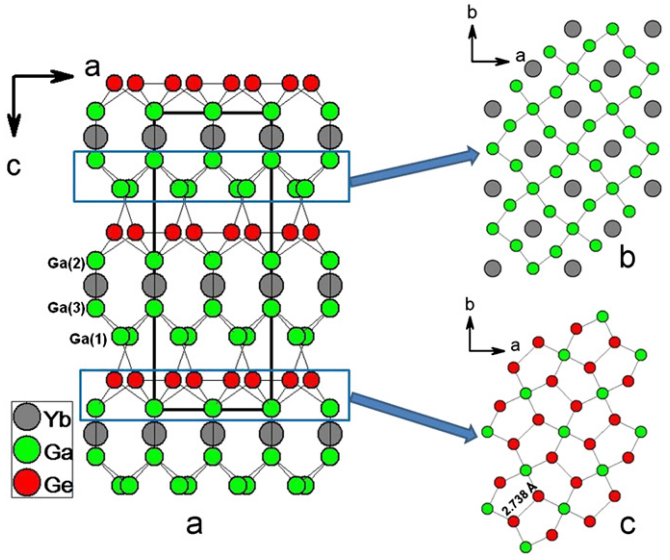

Fig. 5. (a) The non-centrosymmetric structure of $YbGa_4Ge_2$ viewed down the *b*-axis. (b) The puckered Ga layer forms a distorted two-dimensional quadratic sheet that extends in the *ab*-plane. (c) The Ga and Ge layer is defined by fused 5-membered rings along the *ab* plane.

The local coordination polyhedral of Yb (within 3.5 Å) and Ga and Ge atoms (within 3.0 Å) are shown in supporting information. Bonds to the Yb atoms have been omitted to emphasize the three-dimensional framework and its channels. The Yb atom is located in the center of a cage consisting of twelve Ga and two Ge atoms. The Yb–Ga bond lengths in $YbGa_4Ge_2$ vary from 3.155(15) to 3.270(2) Å. Similar Yb–Ga bonding interactions were observed for other compounds in the Yb–Ga–Ge system [11,20].

The Ga(1) atom is found in a three-coordinate trigonal geometry. The Ga(2) and Ga(3) atoms are 5-coordinate and have square pyramidal geometry. Ge is found in a tetrahedral geometry. The shortest interatomic distance is between Ge and Ga(1), which is 2.478(4) Å and is equal to the sum of the covalent radii of Ga and Ge (2.48 Å) [46]. This value is similar to Ga–Ge distances in other compounds such as CaGaGe (2.502 Å), $EuGa_2Ge_4$ (2.489 Å) and $Yb_3Ga_4Ge_6$ (2.504 Å). However, the shortest Ge–Ge distance, 2.738(4) Å, is much larger than the sum of the covalent radii for two Ge atoms (2.44 Å) [46] and the Ge–Ge distances found in elemental Ge (2.45 Å) [44], $Yb_2Ga_4Ge_6$ (2.505 Å) and $Yb_3Ga_4Ge_6$ (2.489 Å) [11].

3.3. Physical properties

The molar magnetic susceptibility (χ) as a function of temperature (T) is shown in Fig. 6. $\chi(T)$ increases with decreasing temperature and does not exhibit any magnetic transition in the entire temperature range from 2 to 300 K. The plot of inverse susceptibility (χ^{-1} vs. T) is continuously changing and does not exhibit any linear region. This indicates the strong influence of crystal field effect on the ground state. The susceptibility data was fitted to the modified Curie–Weiss law, given as

$$\chi = \chi_0 + \frac{C}{(T-\theta_p)}$$

where χ_0 is the temperature independent Pauli contribution, C is the Curie constant and θ_p is the paramagnetic Curie temperature. From the value of C, the effective Bohr magneton number, μ_{eff}, calculated is 1 μ_B/fu, which corresponds to 0.57 μ_B/Yb ion. The inset in Fig. 6 exhibits the magnetization measured as a function of fields up to 50 kOe. Two noticeable observations from this figure are (a) the non-linear behavior of $M(H)$ and (b) the low values of moment and non-saturation of $M(H)$ up to 50 kOe. These observations indicate degenerate ground state due to crystalline electric field effect (CEF).

In Fig. 7, resistivity (ρ) measured in zero field is shown as a function of temperature. The metallic nature of $Yb_3Ga_7Ge_3$ is clearly evident from the feature of $\rho(T)$. Resistivity is continuously decreasing with decreasing temperature. At low temperatures, the $\rho(T)$ data can be fitted to the power-law function, $\rho = \rho_0 + AT^n$, where ρ_0 is the residual resistivity expressed in units of μΩ cm, A and n are the fitting parameters. The values obtained from the fit are shown in Fig. 7. According to the Fermi-liquid theory, at low temperatures, the resistivity varies as $\rho = \rho_0 + AT^2$. Experimentally it has been observed that when electron–electron scattering dominates over electron–phonon scattering, $\rho \propto T^2$. The value obtained from the fit of power-law is close to 2, which is the case for systems exhibiting Fermi liquid state [47]. In order to verify this for $Yb_3Ga_7Ge_3$, the resistivity data is plotted as $(\rho - \rho_0)$ vs. T^2 as inset to Fig. 7. The linearity of the data shows that the compound $Yb_3Ga_7Ge_3$ shows Fermi-liquid behavior at low temperatures.

The specific heat of $Yb_3Ga_7Ge_3$ is shown in Fig. 8. $C(T)$ does not exhibit any anomaly and decreases with decreasing temperature. The plot of C/T vs. T^2 is shown as an inset in Fig. 8. The electronic

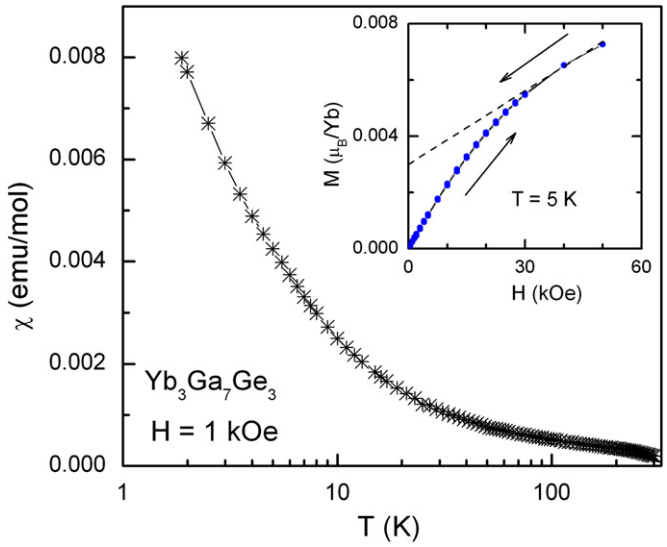

Fig. 6. Magnetic susceptibility ($\chi = M/H$) of $Yb_3Ga_7Ge_3$ measured in a field of 1 kOe is plotted as a function of temperature (on log scale). The magnetization as a function of field measured at $T = 5$ K is shown in the inset. The arrows indicate the direction of the field. A dashed line is drawn to show the non-linearity of the $M(H)$ curve.

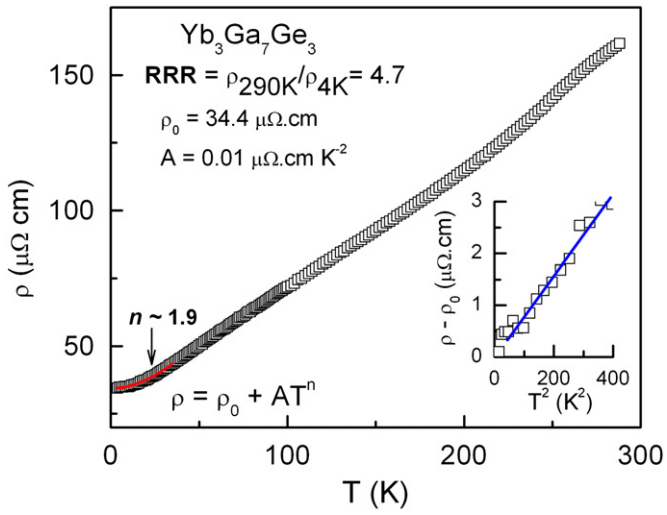

Fig. 7. Resistivity (ρ) measured as a function of temperature. The low temperature data has been fitted to the power law, $\rho = \rho 0 + AT^n$. The values obtained from the fit are shown in the figure. In order to verify the Fermi liquid behavior in $Yb_3Ga_7Ge_3$ the plot of $\rho - \rho_0$ vs. T^2 is shown as an inset. The blue line passing through the data points in the inset figure is drawn as a guide to the eye only, to show the linearity of the data. (For interpretation of the references to color in this figure legend, the reader is referred to the web version of this article.)

coefficient of specific heat, also known as the Sommerfeld coefficient (γ) obtained in the temperature range 5–14 K, from the fit of the form, $C/T = \gamma + \beta T^2$ yields the value of $\gamma = 6.85$ mJ/mol K^2 and the lattice contribution to the specific heat, $\beta = 1.44$ mJ/mol K^4, correspondingly the Debye temperature, $\Theta_D = (12\pi^4 Rn/5\beta)^{1/3} = 110$ K, where R is the gas constant, and n is the number of atoms in the formula unit. The low value of γ rules out any heavy fermion behavior in $Yb_3Ga_7Ge_3$.

4. Concluding remarks

The centrosymmetric $Yb_3Ga_7Ge_3$ and polar $YbGa_4Ge_2$ were obtained from reactions in molten Ga over a relatively broad

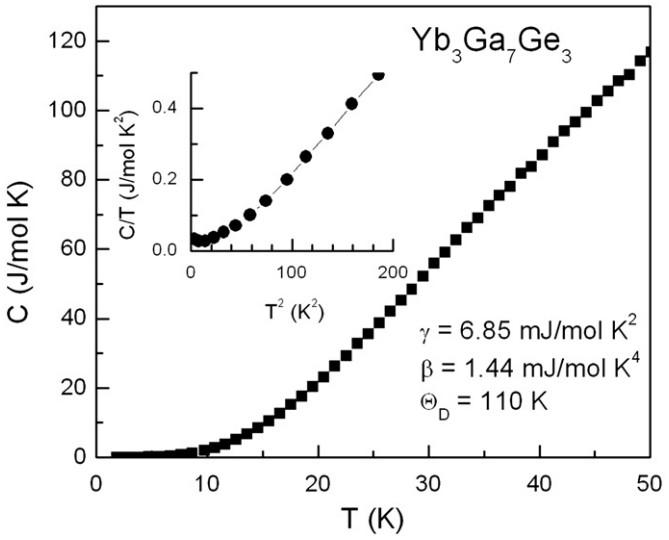

Fig. 8. Specific heat is plotted as a function of temperature for $Yb_3Ga_7Ge_3$. The data is plotted as C/T vs. T^2 as inset, to determine the values of electronic coefficient of specific heat, γ and β which is the lattice contribution to C, in the temperature range of 5–14 K. The Debye temperature (Θ_D) calculated from the β value is also shown in the figure.

range of synthetic conditions. The flux method proves to be an excellent tool for discovering new intermetallic compounds with complex crystal structures. The single crystal neutron diffraction studies performed on $Yb_3Ga_7Ge_3$ showed that two Ga and one Ge atoms are fully occupied and three sites are partially occupied with Ge atoms. The close structural relationship of $Yb_3Ga_7Ge_3$ and Yb_3Ga_9Ge suggests they are two members of the same family with different structure type within a broad stoichiometric width of $Yb_3Ga_{10-x}Ge_x$ and therefore more compositions with similar or new structure types are expected as a function of x. The physical properties of $Yb_3Ga_7Ge_3$ point to a Fermi-liquid regime at low temperature as $\rho \propto T^2$. However, it should be cautioned here that our assessment of $Yb_3Ga_7Ge_3$ is based on our experiments in a limited temperature range of 2–300 K. Therefore it is necessary to study this compound in great detail using various experimental tools such as neutron scattering, ^{170}Yb Mössbauer spectroscopy. Carrying out specific heat, resistivity measurements under applied magnetic field and also down to sufficiently low temperature (milli-Kelvin range) would yield wealth of information in understanding the actual ground state of this compound and also to elucidate the role of valence fluctuation or degeneracy with regard to Fermi-liquid regime in $Yb_3Ga_7Ge_3$.

Supporting information available

Anisotropic displacement parameters, local coordination of atoms, powder diffraction patterns and crystal structure of $Yb_3Ga_7Ge_3$ in the *ac* plane. This material is available free of charge via the Internet at http://pubs.acs.org.

Acknowledgments

Research at Argonne is supported by the US Department of Energy, Office of Science, Office of Basic Energy Sciences, Materials Sciences and Engineering Division (Argonne Contract No. DE-AC02-06CH11357). Use was made of facilities operated by the Northwestern Materials Research Center under NSF Grant

DMR-0520513. Technical support on the PPMS at Northwestern University was provided by Dr. O. Chernyashevskyy.

References

[1] M.G. Kanatzidis, R. Pottgen, W. Jeitschko, Angew. Chem.-Int. Ed. 44 (2005) 6996–7023.
[2] P.H. Tobash, S. Bobev, J.D. Thompson, J.L. Sarrao, J. Alloys Compd. 488 (2009) 533–537.
[3] S. Bobev, J. Hullmann, T. Harmening, R. Pottgen, Dalton Trans. 39 (2010) 6049–6055.
[4] A.C. Payne, A.E. Sprauve, M.M. Olmstead, S.M. Kauzlarich, J.Y. Chan, B.A. Reisner, J.W. Lynn, J. Solid State Chem. 163 (2002) 498–505.
[5] E.M. Benbow, S.E. Latturner, J. Solid State Chem. 179 (2006) 3989–3996.
[6] J. Jiang, A.C. Payne, M.M. Olmstead, H.O. Lee, P. Klavins, Z. Fisk, S.M. Kauzlarich, R.P. Hermann, F. Grandjean, G.J. Long, Inorganic Chem. 44 (2005) 2189–2197.
[7] A.V. Tkachuk, S.J. Crerar, A. Mar, J. Solid State Chem. 177 (2004) 3939–3943.
[8] J.V. Zaikina, Y.J. Jo, S.E. Latturner, Inorg. Chem. 49 (2010) 2773–2781.
[9] A. Grytsiv, A. Leithe-Jasper, H. Flandorfer, P. Rogl, K. Hiebl, C. Godart, T. Velikanova, J. Alloys Compds. 266 (1998) 7–12;
R. Gumeniuk, E. Bischoff, U. Burkhardt, Y. Prots, W. Schnelle, L. Vasylechko, M. Schmidt, Y. Kuzma, Y. Grin, J. Solid State Chem. 182 (2009) 3374–3382;
R.T. Macaluso, M. Francisco, D.P. Young, S. Stadler, J.F. Mitchell, U. Geiser, H.Y. Hong, M.G. Kanatzidis, J. Solid State Chem. 184 (2011) 3185–3189;
M.C. Menard, Y.M. Xiong, A.B. Karki, B.L. Drake, P.W. Adams, F.R. Fronczek, D.P. Young, J.Y. Chan, J. Solid State Chem. 183 (2010) 1935–1942.
[10] X.Z. Chen, P. Larson, S. Sportouch, P. Brazis, S.D. Mahanti, C.R. Kannewurf, M.G. Kanatzidis, Chem. Mater. 11 (1999) 75–83.
[11] M.A. Zhuravleva, J. Salvador, D. Bilc, S.D. Mahanti, J. Ireland, C.R. Kannewurf, M.G. Kanatzidis, Chem.-a Eur. J. 10 (2004) 3197–3208.
[12] X.Z. Chen, P. Small, S. Sportouch, M. Zhuravleva, P. Brazis, C.R. Kannewurf, M.G. Kanatzidis, Chem. Mater. 12 (2000) 2520–2522.
[13] J.R. Salvador, C. Malliakas, J.R. Gour, M.G. Kanatzidis, Chem. Mater. 17 (2005) 1636–1645.
[14] M.A. Zhuravleva, D. Bilc, R.J. Pcionek, S.D. Mahanti, M.G. Kanatzidis, Inorg. Chem. 44 (2005) 2177–2188.
[15] M. Schluter, W. Jeitschko, Inorg. Chem. 40 (2001) 6362–6368.
[16] A. Lacerda, P.C. Canfield, W.P. Beyermann, M.F. Hundley, J.D. Thompson, G. Sparn, Z. Fisk, C. Burns, D. Barnhart, A.C. Lawson, G.H. Kwei, J. Goldstone, J. Alloys Compd. 181 (1992) 191–196.
[17] Y.P. Yarmolyuk, Y.N. Grin, I.V. Rozhdestvenskaya, O.A. Usov, A.M. Kuzmin, V.A. Bruskov, E.I. Gladyshevsky, Kristallografiya 27 (1982) 999–1001.
[18] Y.N. Grin, Y.P. Yarmolyuk, I.V. Rozhdestvenskaya, Kristallografiya 28 (1983) 806–808.
[19] Y.N. Grin, Y.P. Yarmolyuk, V.E. Zavodnik, Kristallografiya 29 (1984) 228–231.
[20] M.A. Zhuravleva, M.G. Kanatzidis, J. Solid State Chem. 173 (2003) 280–292.
[21] M. Schluter, W. Jeitschko, Z. Anorg. Allg. Chem. 626 (2000) 2217–2222.
[22] M.A. Zhuravleva, M.G. Kanatzidis, Inorg. Chem. 47 (2008) 9471–9477.
[23] M.A. Zhuravleva, X.P. Wang, A.J. Schultz, T. Bakas, M.G. Kanatzidis, Inorg. Chem. 41 (2002) 6056–6061.
[24] M.A. Zhuravleva, X.Z. Chen, X.P. Wang, A.J. Schultz, J. Ireland, C.K. Kannewurf, M.G. Kanatzidis, Chem. Mater. 14 (2002) 3066–3081.
[25] M.A. Zhuravleva, M.G. Kanatzidis, Z. Naturforsch. B-a J. Chem, Sci. 58 (2003) 649–657.
[26] M.A. Zhuravleva, R.J. Pcionek, X.P. Wang, A.J. Schultz, M.G. Kanatzidis, Inorg. Chem. 42 (2003) 6412–6424.
[27] D.L. Gray, M.C. Francisco, M.G. Kanatzidis, Inorg. Chem. 47 (2008) 7243–7248.
[28] Y. Matsumoto, S. Nakatsuji, K. Kuga, Y. Karaki, N. Horie, Y. Shimura, T. Sakakibara, A.H. Nevidomskyy, P. Coleman, Science 331 (2011) 316–319.
[29] S. Ernst, S. Kirchner, C. Krellner, C. Geibel, G. Zwicknagl, F. Steglich, S. Wirth, Nature 474 (2011) 362–366.
[30] O. Stockert, J. Arndt, E. Faulhaber, C. Geibel, H.S. Jeevan, S. Kirchner, M. Loewenhaupt, K. Schmalzl, W. Schmidt, Q. Si, F. Steglich, Nat. Phys. 7 (2011) 119–124.
[31] J.R. Salvador, F. Gu, T. Hogan, M.G. Kanatzidis, Nature 425 (2003) 702–705.
[32] F.R. Drymiotis, Y. Lee, G. Lawes, J.C. Lashley, T. Kimura, S.M. Shapiro, A. Migliori, V. Correa, R.A. Fisher, Phys. Rev. B 71 (2005).
[33] A. Iandelli, Z. Anorg. Allg. Chem. 330 (1964) 221–232.
[34] I.S. X-AREA, STOE & Cie GmbH, Darmstadt, 2006.
[35] V. Petricek, M. Dusek, L. Palatinus, Jana 2006, Institute of Physics, Praha, Czech Republic, 2006.
[36] A.J. Schultz, P.M. De Lurgio, J.P. Hammonds, D.J. Mikkelson, R.L. Mikkelson, M.E. Miller, I. Naday, P.F. Peterson, R.R. Porter, T.G. Worlton, Phys. B-Condens. Matter 385–386 (2006) 1059–1061.
[37] A.J. Schultz, R.L. Carlin, Acta Crystallograph. Sect. B-Struct. Sci. 51 (1995) 43–47.
[38] D. Mikkelson, A.J. Schultz, R. Mikkelson, T. Worlton, in: S.C. Billinge, L. Cranswick, R. Lifshitz (Eds.), IUCR Commision on Crystallographic Computing Newsletter, 2005.
[39] V.F. Sears, Methods of Experimental Physics, Academic Press, Orlando, FL, 1986. vol. 23, pp. 521–550..
[40] A.C. Larson, R.B. Von Dreele, General Structure Analysis System—GSAS, Los Alamos National Laboratory, 2000.
[41] P. Debye, Ann. Phys. 39 (1912) 789.
[42] I. Todorov, D.Y. Chung, L.H. Ye, A.J. Freeman, M.G. Kanatzidis, Inorg. Chem. 48 (2009) 4768–4776.
[43] C.P. Sebastian, M.G. Kanatzidis, J. Solid State Chem. 183 (2010) 2077–2081.
[44] L. Pauling, The Nature of the Chemical Bond, third ed., Cornel University Press, Ithaca, NY, 1960., p. 410.
[45] Y. Tagawa, J. Sakurai, Y. Komura, T. Ishimasa, J. Less-Common Met. 119 (1986) 269–275.
[46] G. Wulfsberg, Inorganic Chemistry, University Science Books, Sausalito, CA, 2000. p 32.
[47] C.M. Varma, Rev. Mod. Phys. 48 (1976) 219.